Available online at www.sciencedirect.com

SCIENCE DIRECT®

Biochimica et Biophysica Acta 1657 (2004) 47–60

BIOCHIMICA ET BIOPHYSICA ACTA

BBA

www.bba-direct.com

Correlation between lifetime heterogeneity and kinetics heterogeneity during chlorophyll fluorescence induction in leaves: 2. Multi-frequency phase and modulation analysis evidences a loosely connected PSII pigment–protein complex

Nicolae Moise*, Ismaël Moya

Laboratoire pour l'Utilisation du Rayonnement Electromagnétique, Centre Universitaire Paris-Sud, Bat. 209D, B.P. 34, 91898 Orsay Cedex, France

Received 28 November 2003; received in revised form 17 March 2004; accepted 1 April 2004
Available online 22 April 2004

Abstract

We report the first direct decomposition of the fluorescence lifetime heterogeneity during multiphasic fluorescence induction in dark-adapted leaves by multi-frequency phase and modulation fluorometry (PMF). A very fast component, assigned to photosystem I (PSI), was found to be constant in lifetime and yield, whereas the two slow components, which are strongly affected by the closure of the reaction centers by light, were assigned to PSII. Based on a modified "reversible radical pair" kinetic model with three compartments, we showed that a loosely connected pigment complex, which is assumed to be the CP47 complex, plays a specific role with respect to the structure and function of the PSII: (i) it explains the heterogeneity of PSII fluorescence lifetime as a compartmentation of excitation energy in the antenna, (ii) it is the site of a conformational change in the first second of illumination, and (iii) it is involved in the mechanisms of nonphotochemical quenching (NPQ). On the basis of the multi-frequency PMF analysis, we reconciled two apparently antagonistic aspects of chlorophyll *a* fluorescence in vivo: it is heterogeneous with respect to the kinetic structure (several lifetime components) and homogeneous with respect to average quantities (quasi-linear mean $\tau-\Phi$ relationship).

Keywords: Chlorophyll *a* fluorescence induction; $\tau-\Phi$ relationship; Photochemical and thermal phase; PSII energy transfer kinetic model; PSII pigment–protein complex; Conformational change

1. Introduction

Fluorescence lifetime measurements using time-correlated single-photon counting (TCSPC) and picosecond laser excitation have been extensively applied to investigate the fluorescence heterogeneity of photosynthetic systems from higher plants. Measured at steady states, F_o, F_m or F_s, the fluorescence emission of chlorophyll (Chl) *a* has been found to be heterogeneous [1–6]. The results obtained by various groups differ in terms of the number of the fluorescence decay components and the associated lifetimes and amplitudes. However, these groups generally agree on the main components. In addition to photosystem I (PSI) and photosystem II (PSII) fluorescence heterogeneity, the problem of assigning each fluorescence decay component to a structural and functional part of the photosynthetic systems has frequently been related to PSII heterogeneity and is still under debate [5–10]. The most relevant structural and functional PSII heterogeneities seem to be (i) the antenna-size heterogeneity [11] with PSII α (major fraction, larger antenna, high connectivity) and PSII β (minor fraction, smaller antenna, low connectivity) and (ii) the heterogeneity

Abbreviations: Chl, chlorophyll; OIDPSMT, nomenclature for Chl *a* fluorescence induction; OI, photochemical phase; IP, thermal phase; F_o, minimal fluorescence level; F_m, maximal fluorescence level in dark-adapted leaves under saturating actinic light; F_p, fluorescence peak in dark-adapted leaves under low actinic light; F_s, steady-state fluorescence level; DCMU, 3-(3,4-dichlorophenyl)-1,1-dimethylurea; PSI, photosystem I; PSII, photosystem II; PQ, plastoquinone; Q_A, primary quinone electron acceptor of PSII; Q_B, second quinone electron acceptor of PSII; LHCII, light-harvesting complex of PSII; NPQ, nonphotochemical quenching; RRP model, "reversible radical pair" model; PMF, phase and modulation fluorometry; TCSPC, time-correlated single-photon counting; PMT, photomultiplier tube

* Corresponding author. Tel.: +33-1-64-46-80-54; fax: +33-1-64-46-80-07.
E-mail address: nicolae.moise@lure.u-psud.fr (N. Moise).

0005-2728/$ - see front matter © 2004 Elsevier B.V. All rights reserved.
doi:10.1016/j.bbabio.2004.04.003

of the Q_B non-reducing centers with respect to electron transfer from Q_A to Q_B [12,13]. PSII heterogeneity has been described in detail [14–16]. The picture of PSII α and PSII β heterogeneity has been widely used in fluorescence lifetime analysis [4,6–8,17,18] but also criticized [1,9].

Attempts were made to establish correlations between fluorescence lifetime and yield parameters during the fast changes in fluorescence. A dark-to-light transition induces a typical variation of the Chl *a* fluorescence called "fluorescence induction" and denoted OIDPSMT [19,20]. It consists of a fast fluorescence rise from O, minimal fluorescence, to P, maximal fluorescence, in the first second of illumination, and a slow decrease within minutes from P to a steady state (S or T). Since the TCSPC method is time-consuming, one difficulty was to maintain constant the intermediate states of the fluorescence induction long enough to measure the fluorescence lifetime with sufficient precision. To obtain intermediate levels between the minimal and maximal fluorescence yield, several methods have been employed. First, a variable number of closed PSII reaction centers can be obtained by varying the concentrations of inhibitors like DCMU or atrazine [5,10,21]. However, it is worth noting that these measurements are affected by the quenching of oxidized PQs [22]. In addition, the inhibition by herbicides could be incomplete, at least in leaves, and could lead to high spatial heterogeneity of Chl fluorescence.

A second approach employed to produce different levels of fluorescence yield and lifetime in thylakoids and algae suspensions was based on the flow method [23]. By varying the flow rate of the sample, and thus the illumination duration, the measured fluorescence corresponds to a continuously varying mixture of different yield values ranging from the minimal to the maximal fluorescence induction levels [24]. Therefore, this method leads to ambiguous lifetime decomposition. In a third technique, the intermediate fluorescence yield values are obtained by pretreating the sample with different actinic light intensities before the measurements [9,24–28]. In this case, fluorescence levels correspond to the slow PS phase rather than to the fast OIP phase of fluorescence induction. All of these techniques generate pseudo-stationary states, which do not correspond to the real intermediate states of the OIP fluorescence induction phase.

We report in this study the first direct decomposition of Chl *a* fluorescence lifetime heterogeneity during the OIDPSMT multiphasic fluorescence induction in leaves using the method of multi-frequency phase and modulation fluorometry (PMF). This approach allows the fluorescence phase and modulation factors to be measured with a millisecond sampling rate and, accordingly, to obtain the fluorescence induction kinetics of yield and lifetime in a direct manner. The measured intermediate states correspond to the real closure of PSII reaction centers during the fluorescence induction and are free of the difficulties stated above. The results obtained from the multi-frequency PMF analysis strengthen the hypothesis of a conformational change during the IP thermal phase of the fluorescence induction, proposed in the companion paper (N. Moise and I. Moya, Correlation between lifetime heterogeneity and kinetics heterogeneity during chlorophyll fluorescence induction in leaves: 1. Mono-frequency phase and modulation analysis reveals a conformational change of a PSII pigment complex during the IP thermal phase), and show that this conformational change mainly affects the slowest PSII lifetime component. The fluorescence lifetime heterogeneity is interpreted within the framework of a modified "reversible radical pair" (RRP) kinetic model with three compartments. A loosely connected antenna compartment, which accounts for the lifetime heterogeneity, is involved in the conformational change and nonphotochemical energy dissipation. Evidence is provided to identify this compartment as the CP47 complex of the PSII core antenna.

2. Materials and methods

2.1. Plant material

Prunus laurocerasus leaves were used for a direct analysis of the fluorescence lifetime heterogeneity during the entire fluorescence induction OIDPSMT. The leaves were harvested from a plant grown outdoors in Orsay (France) and were dark-adapted for 1 h prior to the measurements.

2.2. Multi-frequency cross-correlation PMF

In this work, a multi-frequency phase and modulation fluorometer based on the cross-correlation technique [29,30] was developed. This type of instrument offers high sensitivity, low noise and high accuracy in the phase and modulation determination as a result of low bandwidth detection (high-to-low frequency translation). Fig. 1 illustrates the experimental set–up. The fluorescence was induced by a 635-nm laser diode (Hitachi HL 6320G, 10 mW; Optilas, Evry, France) controlled by a high frequency signal generator (Hewlett Packard HP 8648 A; Les Ulis, France). The optical modulation factor was better than 95% in the range of 10 MHz to 1 GHz. The emitted fluorescence was focused by a bi-convex lens onto the entrance slit of the H10 monochromator (f/3.5 aperture, 8 nm bandpass; Jobin Yvon, Longjumeau, France). The exit slit of the monochromator was imaged on a red sensitive photomultiplier tube (PMT) detector (Hamamatsu H5023, S20 photocathode, 500 MHz bandpass; Japan) by an optical system of two plano-convex lenses. All lenses were protected with broadband antireflection coatings. A long-pass 665-nm filter (Schott RG 665, 4 mm; Clichy, France) was used to suppress the scattered laser excitation light from the fluorescence emission. To avoid thermal drift, the temperature of the PMT was maintained constant. Although the system was designed to separate the fluorescence emission spectrally, we used the

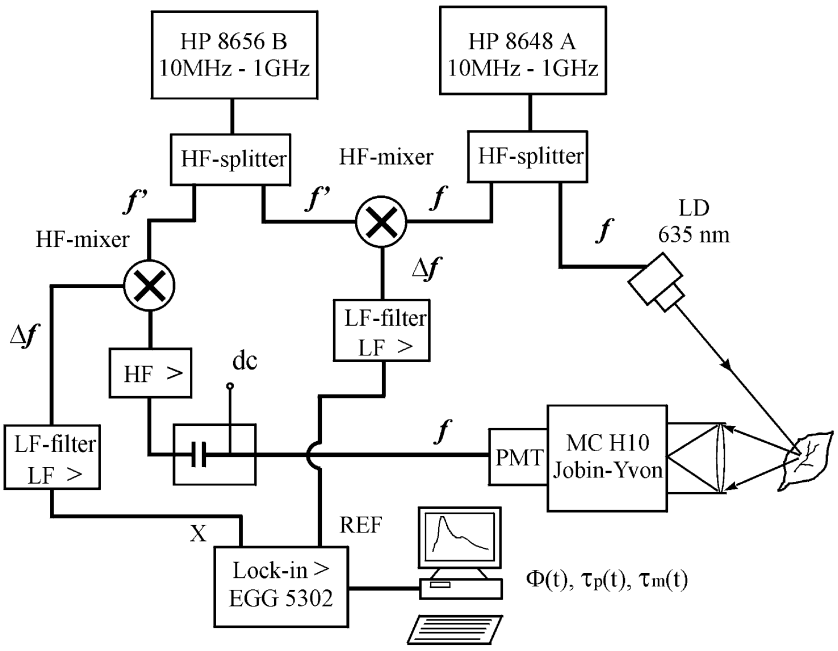

Fig. 1. Experimental set-up of the multi-frequency PMF instrument. The laser diode (LD) excitation at 635 nm is modulated at the frequency (f) in the range of 30 to 500 MHz. The modulated fluorescence signal supplied by the PMT detector is externally cross-correlated by a second modulated signal at the frequency ($f'=f+\Delta f$). To improve the stability, the two frequency synthesizers were phase-locked. The fluorescence phase and modulation information is translated from high-to-low frequency (Δf) and then detected by a lock-in amplifier (X-signal, REF-reference). Three signals are acquired, namely the fluorescence (dc) component, the fluorescence phase (ϕ) and the modulation (m). At each frequency, the induction curves of the fluorescence yield (Φ) and the phase and modulation lifetimes (τ_p and τ_m) are obtained with a millisecond-sampling rate.

monochromator in the zero order in this work to improve the signal-to-noise ratio.

The cross-correlation detection requires the use of two frequencies (f, f'), with a precise and stable difference Δf (usually from 1 to 1000 Hz) between them over the entire frequency range of measurements. The output of a second generator (Hewlett Packard HP 8656B; Les Ulis, France) was used to cross-correlate the PMT anode signal. This required external mixing, RF and LF-amplification, filtering and RF-shielding, as shown in Fig. 1. To obtain the integrated (dc) fluorescence intensity, an inductor was added before the mixer in a 50-Ω adapted circuit. Furthermore, the (dc) component was decoupled before input to the mixer. The reference signal of the lock-in amplifier was obtained by the cross-correlation method in a similar manner. As our main goal was to measure fluorescence lifetime variations with a millisecond-sampling rate, the frequency of the cross-correlation signal was set at 5 kHz. Phase and modulation parameters of the cross-correlation signal were measured by a PAR 5202 lock-in amplifier (EGG, Princeton Applied Research, USA), whose time constant was set at 100 μs to ensure fast measurements of the fluorescence lifetimes. The acquisition of these signals with three digital multimeters (Hewlett Packard HP 34401A; Les Ulis, France) set the final sampling rates of the entire system at 700 μs for 512 points (to investigate the OIP fluorescence phase) or 15 ms for a few thousand points (to investigate mainly the PS slow decay phase).

Excitation of a sample with sinusoidally modulated light results in the re-emission of sinusoidally modulated fluorescence at the same frequency as the excitation, but shifted in phase and demodulated in amplitude. By measuring the phase (ϕ) and demodulation factor (m), we can calculate the fluorescence phase (τ_p) and modulation (τ_m) lifetime at each modulation frequency according to Eq. (A6) [29]. Two different dyes on a solid support with calibrated lifetimes of 0.5 and 2.25 ns, respectively, were used as references for the determination of the phase and modulation. Measuring the phase and modulation of the sample with respect to a fluorophore of known lifetime and similar fluorescence spectrum rather than to a scatterer allows the timing errors due to the time-response of PMT on the incident wavelength to be minimized [31]. The maximal errors of our instrument in the phase and modulation determination were limited at 0.2° and 0.005, respectively. These values are currently reported for many other instruments based on the cross-correlation technique. The specificity and originality of our instrument lies in its millisecond time response, thus allowing lifetime measurements even during rapid fluorescence changes.

2.3. Fluorescence lifetimes analysis

Fluorescence inductions were performed at 12 modulation frequencies (30, 54, 80, 100, 170, 210, 260, 310, 360, 400, 450, 500 MHz) at average light intensities of approx-

imately 70 μmol photons m^{-2} s^{-1} on dark-adapted leaves. The OIP induction transients of the fluorescence yield Φ, the phase τ_p and modulation τ_m lifetimes were obtained at each modulation frequency. The extended frequency range provides a good resolution for the retrieval of the multi-exponential decays. The duration of each illumination was only 1.6 s, long enough for the variable fluorescence to reach its peak value. A time interval of about 15–20 min for the dark readaptation of the plants was left between two consecutive inductions. We emphasize that reproducibility of the fluorescence induction curves is a prerequisite for accurate multi-frequency analysis. This is difficult to achieve when working with intact leaves and experiments at long duration (3 to 4 h) and is the main source of error in the multi-frequency PMF analysis. However, the errors originating from repeat measurements on the same sample were comparable to those of the synthetic data used to test the decomposition program (Appendix A).

A multi-frequency analysis during the slow PS phase of the fluorescence induction was also performed but only at three modulation frequencies (54, 200 and 500 MHz) because the reproducibility of this phase is even more difficult to achieve. This phase is sensitive to the environmental conditions and is controlled by antagonistic factors that frequently lead to non-reproducible oscillations. However, three different modulation frequencies are sufficient to resolve a heterogeneous system with three components [32].

The procedure for the analysis of the multi-frequency PMF data is described in detail in Appendix A. Each point of the fluorescence induction is independent and is characterized by a fluorescence yield value (Φ) and by ($2 \times N$) values of the PMF lifetimes (τ_p and τ_m), where N is the number of modulation frequencies. The parameters obtained at a particular point of the fluorescence induction by the decomposition program are used as initial values for the following point.

The parameters obtained after a complete analysis represent the heterogeneity of the fluorescence emission during the entire fluorescence induction. The capability of the fitting program to determine the lifetime components has been successfully checked using synthetic data in the presence of a noise level higher than expected in our experimental data (Appendix A).

3. Results

3.1. Measurements of multi-frequency PMF lifetimes

The insets of Fig. 2 show the OIP kinetics of the fluorescence yield (Φ), the phase (τ_p) and modulation (τ_m) lifetimes at two extremes of the modulation frequency (54 and 500 MHz). In addition, the related $\tau-\Phi$ relationships are plotted. At 54 MHz, the $\tau-\Phi$ relationship displays the same features as those obtained with the mono-frequency PMF set-up (see the companion paper): linear during the OI photochemical phase that does not extrapolate to zero, followed by an upward (convex) curvature during the IP thermal phase (Fig. 2A). At higher modulation frequencies, the τ_p and τ_m lifetimes are markedly reduced. For instance, at the P maximum of the induction curve, τ_p and τ_m decrease from 1.85 and 2.22 ns at 54 MHz (Fig. 2A) to only 0.6 and 1.6 ns at 500 MHz (Fig. 2B), respectively. The decrease of the lifetime when increasing the frequency is a consequence of the preferential damping of longer lifetime components [29]. In phase fluorometry, high modulation frequencies are suitable to retrieve short lifetime components, whereas low frequencies are more adapted for long lifetimes. Most importantly, both the $\tau_p-\Phi$ and $\tau_m-\Phi$ relationships are linear during the IP phase at 500 MHz (Fig. 2B). This result suggests that the convex curvature is due to the contribution of a long lifetime component that is damped at high modulation frequencies. Measurements at frequencies between 54 and 500 MHz led to intermediary τ_p and τ_m lifetime curves (data not shown).

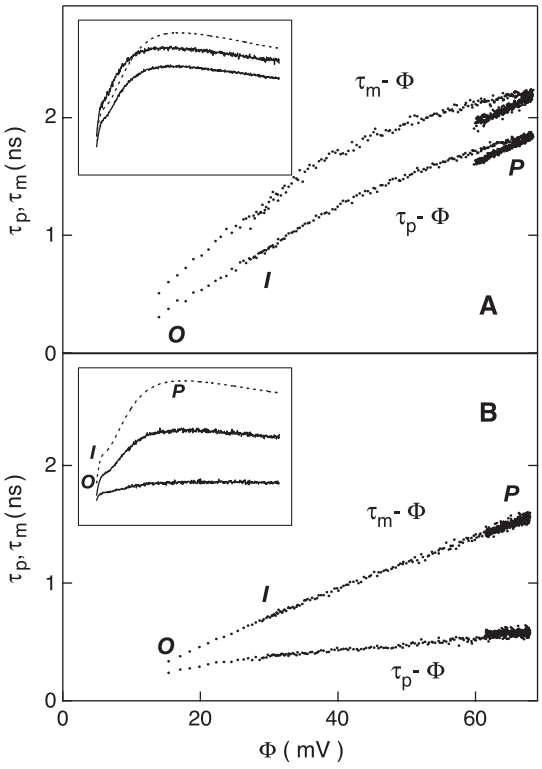

Fig. 2. $\tau-\Phi$ relationships measured during the OIP phase of the fluorescence induction on a *P. laurocerasus* leaf at: (A) 54 MHz, (B) 500 MHz. The intensity of the actinic light was 70 μmol photons m^{-2} s^{-1}. The insets show the OIP induction curves of the yield Φ (dashed curve) and lifetimes τ_p and τ_m (solid curves with $\tau_m > \tau_p$).

PMF measurements at three modulation frequencies between 54 and 500 MHz were also performed during the slow PS phase of the fluorescence induction. Irrespective of the modulation frequency, the $\tau-\Phi$ relationships of τ_p and τ_m were linear during this phase, in agreement with the results of the mono-frequency PMF analysis (see the companion paper).

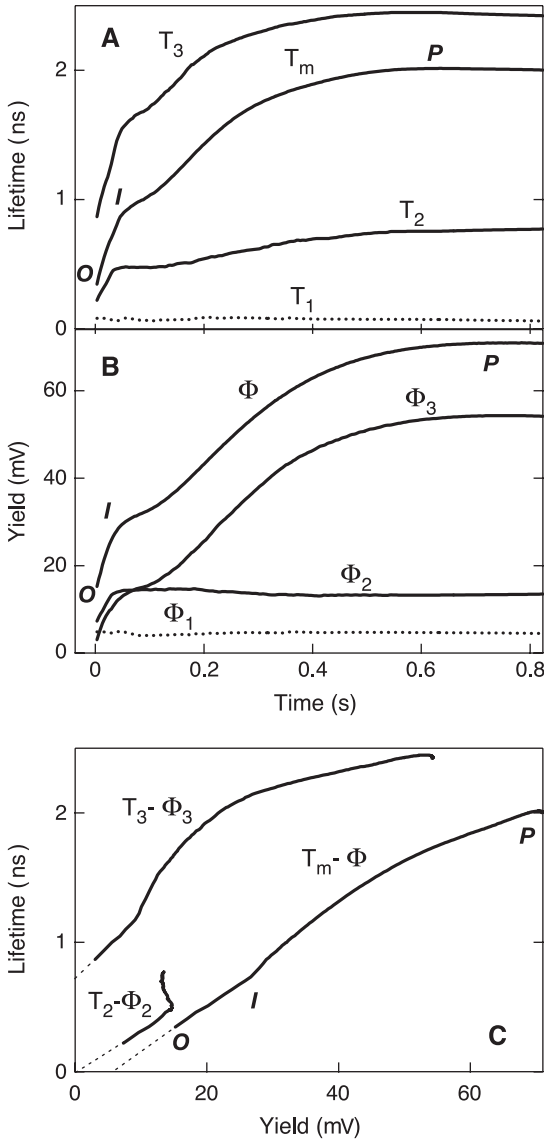

Fig. 3. Analysis of PMF data obtained at 12 modulation frequencies between 30 and 500 MHz during the OIP fluorescence induction phase. A model with three free running components was used to account for the fluorescence lifetime heterogeneity. The picosecond component (T_1, Φ_1), constant in lifetime and yield, was assigned to the PSI emission, whereas the two nanosecond components (T_2, Φ_2 and T_3, Φ_3) were assigned to the variable PSII emission. T_m is the mean lifetime and Φ is the total fluorescence yield. (A) Lifetime kinetics. (B) Yield kinetics. (C) $\tau-\Phi$ relationships of the PSII nanosecond components and mean lifetime.

3.2. Decomposition of multi-frequency PMF lifetimes during the OIP phase

The PMF lifetimes of the OIP fluorescence rise obtained at 12 modulation frequencies were analyzed on the basis of a multi-exponential model with three independent components. Fig. 3 summarizes the results of the data decomposition. We found that a three-exponential model accurately describes the fluorescence heterogeneity during the induction. A four-exponential model was also tested, but two of the components tended to collapse.

The fluorescence lifetime components are labeled T_1, T_2 and T_3, respectively. Their kinetics during the fluorescence induction are shown in Fig. 3A. Upon decomposition, we found that T_1 shows a quasi-constant value of about 70–80 ps, whereas T_2 and T_3 are significantly modified during the variable fluorescence. At the F_o level (O point), T_2 and T_3 have values of 220 and 870 ps, respectively. The closing of PSII reaction centers by light gradually increases the values of T_2 and T_3 at the F_p level (P point) to 780 ps and 2.45 ns, respectively. One can notice that these two components increase almost in parallel during the OI photochemical phase. On the contrary, during the IP thermal phase, T_2 displays a more pronounced plateau than T_3, which is followed by a smaller and lower lifetime increase.

Fig. 3B shows the kinetics of the fluorescence yield of each component (Φ_1, Φ_2 and Φ_3) during the fluorescence induction. In addition, the total fluorescence yield ($\Phi=\Phi_1+\Phi_2+\Phi_3$) is also plotted. Similarly to the lifetimes, only the fluorescence yield of the T_2 and T_3 components (Φ_2 and Φ_3) are affected by the redox state of the PSII reaction centers, whereas the yield of the T_1 component, Φ_1, remains constant throughout the whole fluorescence induction. The transition from O to P changes the contribution of each component to the total fluorescence (fractional intensities) from 30%, 45% and 25% to 6.5%, 19% and 74.5% for T_1, T_2 and T_3, respectively. Notably, the variable fluorescence leads to a more than 17-fold increase of the yield of Φ_3, whereas Φ_2 shows only a twofold yield increase. This huge variation in the yield of the long lifetime component between the F_o and F_p fluorescence levels has already been observed in TCSPC measurements [5,17,21,27,28,33]. In contrast to Φ_3, Φ_2 displays a rapid rise during the OI phase followed by a large plateau and a slow decline during the IP phase. Table 1 summarizes the fluorescence parameters, lifetime and fractional intensity contribution of each fluorescence component at F_o and F_p. These parameters allowed us to calculate the mean fluorescence lifetime, T_m, according to Eq. (A3) (Appendix A). Its time course during the fluorescence induction is shown in Fig. 3A.

Furthermore, the decomposition of the fluorescence emission during the variable fluorescence allowed us to analyze the exact relationship between the lifetime and yield of each component. Therefore, the $\tau-\Phi$ relationships of the

Table 1
Time-resolved fluorescence parameters at the F_o and F_p fluorescence levels obtained upon the direct decomposition of multi-frequency PMF lifetimes measured during the OIP phase of the fluorescence induction

	Lifetime components						Mean lifetime/ Total yield	
	T_1 (ns)	f_1 (%)	T_2 (ns)	f_2 (%)	T_3 (ns)	f_3 (%)	T_m (ns)	Φ (a.u.)
F_o	0.08	30	0.22	45	0.87	25	0.340	15.2
F_p	0.07	6.5	0.78	19	2.45	74.5	1.99	70.8

Twelve modulation frequencies (between 30 and 500 MHz) and a three-independent component model (T_1, T_2 and T_3) were used.

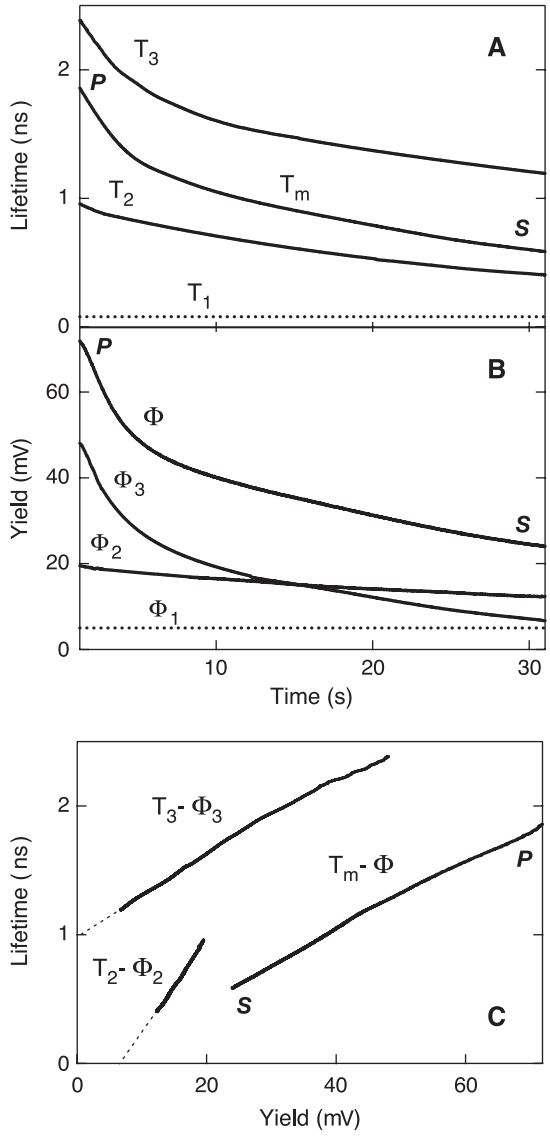

Fig. 4. Analysis of PMF data obtained at three modulation frequencies between 54 and 500 MHz during the PS fluorescence induction phase. A model with three components was used to account for the fluorescence lifetime heterogeneity, one component for the PSI emission (T_1, Φ_1) and two components for the PSII emission (T_2, Φ_2 and T_3, Φ_3). T_1 and Φ_1 were used as known and constant parameters in the decomposition program with values obtained from Table 1. T_m is the mean lifetime and Φ is the total fluorescence yield. (A) Lifetime kinetics. (B) Yield kinetics. (C) $\tau-\Phi$ relationships of the PSII nanosecond components and mean lifetime.

T_2 and T_3 components are shown in Fig. 3C. The most conspicuous effect is seen in the $T_3-\Phi_3$ relationship. This relationship is qualitatively similar to that observed for $\tau_p-\Phi$ and $\tau_m-\Phi$ at 54 MHz: linear during the OI photochemical phase, followed by an important convex curvature during the IP thermal phase. This result clearly shows that the origin of the convex curvature of the mean $\tau-\Phi$ relationship, previously measured with the mono-frequency PMF (see the companion paper), is the T_3 long lifetime component, which itself displays a similar curvature. On the other hand, the $T_2-\Phi_2$ relationship is complicated by the slow decrease of the yield during the IP phase, whereas the lifetime increases. In addition, we note that the linear $T_2-\Phi_2$ relationship during the OI phase extrapolates very close to zero, whereas the extrapolation of the $T_3-\Phi_3$ relationship crosses the lifetime axis at a significant positive value of about 0.7 ns (Fig. 3C).

The values of T_m are intermediate between the lifetimes τ_p and τ_m measured at 54 MHz (from Fig. 3A versus Fig. 2A). The positive intercept of the linear $T_m-\Phi$ relationship on the yield axis (Fig. 3C) agrees well with that obtained for τ_p and τ_m at 54 MHz. More importantly, this contribution corresponds to the yield Φ_1 of the T_1 component obtained by the multi-frequency PMF decomposition of the OIP phase fluorescence.

We finally note that the errors in the determination of the PMF lifetimes with our instrument are much less important than the investigated effect, i.e. the curvature of the $\tau-\Phi$ relationship. This fact reinforces our confidence in the results of the multi-frequency decomposition.

3.3. Decomposition of multi-frequency PMF lifetimes during the PS phase

The results of the multi-frequency PMF analysis performed during the slow PS fluorescence decline are shown in Fig. 4. The results of the OIP fluorescence induction (vide supra) allowed us to introduce the lifetime (80 ps) and yield (corresponding to about 30% of the total fluorescence at F_o) of the T_1 component as known and constant parameters in the decomposition program. This improved the multi-frequency PMF analysis and compensated for the reduced number of measurement frequencies during the PS phase. The lifetimes decreased monotonically from 2.4 to 1.19 ns for T_3 and from 0.96 to 0.4 ns for T_2 (Fig. 4A), whereas the fractional contributions changed from 67% to 29% for T_3 and from 26.5% to 51.5% for T_2 (Fig. 4B). The fluorescence parameters at the F_p and F_s levels, including lifetime and fractional intensity contribution, are summarized in Table 2. The most important result is the linear $\tau-\Phi$ relationship of both T_2 and T_3 components during the entire PS phase (Fig. 4C). Consequently, the $T_m-\Phi$ relationship is also linear (Fig. 4C). The results of the PS phase fluorescence decom-

Table 2
Time-resolved fluorescence parameters at the F_p and F_s fluorescence levels obtained upon the direct decomposition of multi-frequency PMF lifetimes measured during the PS decay phase of the fluorescence induction

	Lifetime components						Mean lifetime/ total yield	
	T_1 (ns)	f_1 (%)	T_2 (ns)	f_2 (%)	T_3 (ns)	f_3 (%)	T_m (ns)	Φ (a.u.)
F_p	0.08	6.5	0.96	26.5	2.4	67	1.87	71.7
F_s	0.08	19.5	0.40	51.5	1.19	29	0.57	24.0

Three modulation frequencies and a three-component model were used. The short lifetime component contribution (T_1), which corresponds to PSI, was assumed known.

position further confirm that the curvature of the $T_3-\Phi_3$ relationship was accurately obtained, i.e., curved during the IP phase and linear during the PS phase according to the behavior of the mean τ_p and τ_m lifetimes at 54 MHz.

It is worth noting that during the PS phase, a significantly positive value of the lifetime was obtained upon extrapolation of the $T_3-\Phi_3$ relationship for all of the samples we examined. In contrast, the $T_2-\Phi_2$ relationship, which is less accurately defined, possibly due to the reduced number of modulation frequencies, did not always extrapolate to zero.

4. Discussion

4.1. The contribution of PSI fluorescence

It is generally assumed that the fluorescence of the PSI antenna is not affected by either the redox state of Q_A or by the redox state of the PSI reaction center [19] and is characterized by a short lifetime [1,2,7,19,34–36]. Based on this hypothesis, the short lifetime component, T_1, characterized by a constant lifetime between 70 and 80 ps and a constant yield during the fluorescence induction, can be clearly assigned to PSI emission. We stress that the results of the multi-frequency analysis provide direct evidence that the fluorescence of PSI is constant.

The relatively high contribution of T_1 found here (30% at F_o and 6–7% at F_p) can be explained by the Chl fluorescence reabsorption in leaves, which tends to enhance the PSI contribution for wavelengths longer than 700 nm [2,34,37]. The constant emission of PSI is also responsible for the positive yield-axis intercept of the $\tau_p-\Phi$ and $\tau_m-\Phi$ relationships obtained with PMF at 54 MHz (Fig. 2A; see also the companion paper). This intercept represents the fluorescence originating from the direct excitation of PSI antenna and agrees well with the fractional contribution of the T_1 component obtained from the multi-frequency PMF decomposition (30% of F_o). Upon removal of the PSI contribution (by using a narrow interference filter centered at 685 nm instead of the wide-band RG 665 filter) the $\tau-\Phi$ relationship extrapolated to zero (see the companion paper). Simulations clearly showed that the contribution of the constant and short lifetime PSI emission led to a similar non-zero extrapolation of the $\tau-\Phi$ relationship [36].

4.2. The contribution of PSII fluorescence

The other two components obtained from the multi-frequency PMF analysis, T_2 and T_3, which have nanosecond lifetimes, are ascribed to the variable fluorescence emission of PSII antenna, since they are strongly affected by closing of the PSII reaction centers in response to light [1,10]. These components represent the commonly observed decays in TCSPC experiments. Moreover, the lifetime and yield values obtained from the multi-frequency PMF decomposition for F_o, F_p and F_s fluorescence are within the range of published values measured by TCSPC fluorometry in leaves [2,34,36,38]. The established fact that two main components in the nanosecond range account for the PSII fluorescence was previously interpreted by some authors to be evidence for different types of PSII units (PSII α and PSII β heterogeneity) [6–8]. In this view, the PSII fluorescence heterogeneity is explained by the superposition of two independent fluorescence emissions. However, this hypothesis has been criticized [1,9], mainly on the basis of similar results obtained on PSII-enriched particles (BBY) that contained only PSII α units.

Different kinetic models have been proposed to take into account the PSII fluorescence heterogeneity. One of them, which is largely used to interpret PSII fluorescence data, is the RRP model [19,39,40]. It is mainly based on two assumptions: (i) upon excitation, an equilibrium is rapidly reached among all PSII antenna pigments and the reaction centers, and (ii) the primary charge separation is reversible in the nanosecond time domain. This model is described by two compartments and predicts a biexponential fluorescence decay with one component in the nanosecond time range and the other in the picosecond time range. It is thus clear that the RRP model as such does not account for the observation of two components with nanosecond lifetimes [38].

To account for both PSII nanosecond lifetime components, we propose a kinetic model in which a third pigment compartment, in incomplete equilibration with the main antenna, is involved (Fig. B1). Such a hypothesis was previously used to explain the fluorescence heterogeneity at the F_o fluorescence level [38,41]. For simplicity, the assumption of the RRP model that the excited states are substantially thermalized before the occurrence of primary photochemical trapping over the entire pigments system was also used in our model, except for the third compartment. The major antenna (LHCII) and the minor antenna are considered to be a single pool of Chl *a*/*b* complexes in the model. This is a reasonable simplification because these Chl *a*/*b* binding complexes are almost isoenergetic [19,42,43].

The kinetic model with three compartments is described in detail in Appendix B. The model incorporates both different rate constants known from the literature and lifetime and yield data obtained by multi-frequency PMF analysis (e.g., data from Table 1 for the F_p fluorescence level). In searching to further reproduce the properties of the third compartment, an inversion kinetic procedure of the model was developed. Using the model at the F_p maximal fluorescence level, we found that the new compartment would account for about 15% of the total light absorption by PSII and its rate constants for energy exchange with the main antenna are small ($k_3 = 0.26$ ns^{-1} and $k_{-3} = 0.2235$ ns^{-1}; Appendix B). These values clearly indicate that the third compartment is loosely connected to the main PSII antenna and, thus, explains the origin of fluorescence lifetime heterogeneity as a compartmentation of excitation

energy among the antenna complexes. In this view, the heterogeneity of the PSII fluorescence lifetime is an intrinsic feature of each PSII unit, irrespective of PSII heterogeneities (e.g., PSII α and PSII β). Our result is a clear indication that the assumption of the original RRP model concerning a fast exciton equilibration within the PSII antenna pigments may be incorrect. To overpass this limitation, individual energy transfer steps between PSII pigment–protein complexes must be explicitly taken into consideration.

The hypothesis of the compartmentation of excitation energy in the antenna agrees well with the recent results of Jennings et al. [44] who found that a component of approximately 30% of the overall trapping time is diffusion-limited and therefore the energy flow into the reaction center complex is rather slow. They concluded that the CP43 and CP47 pigment complexes of the PSII core antenna are intermediary compartments that differentially limit the excitation energy transfer to reaction center. From high-resolution X-ray crystallographic and picosecond fluorescence data, Vasil'ev et al. [45] also showed that the PSII core antenna complexes limit the energy transfer to the reaction center.

Our PSII kinetic model, which naturally generates two nanosecond lifetimes in the experimentally measured range for T_2 and T_3, also generates a third picosecond lifetime component corresponding to the exciton equilibration process. Although this component was not resolved by the multi-frequency PMF analysis, we stress that it has a fractional contribution of only 1.5% (Appendix B) and thus it does not affect the results.

4.3. The OI photochemical phase of fluorescence induction

The concept of the $\tau-\Phi$ relationship, as introduced years ago, concerned only the averaged lifetime, as earlier measurements were unable to resolve the heterogeneity of the fluorescence emission. Earlier studies relied only on the shape of the mean $\tau-\Phi$ relationship to test the validity of a PSII connectivity model. However, this concept is still useful for the individually resolved fluorescence components, as we explain below.

During the OI photochemical phase of fluorescence induction, both PSII fluorescence lifetime components increase almost in parallel. The $\tau-\Phi$ relationships for both PSII lifetime components are linear, suggesting a high degree of co-operativity among the PSII units. The $T_2-\Phi_2$ relationship extrapolates to zero, whereas the $T_3-\Phi_3$ relationship exhibits a significant positive intercept on the lifetime axis at 0.7 ns (Fig. 3C). In order to get additional insight on this striking point, we reviewed the TCSPC lifetime data reported in the literature [1,2,5,6,9,10,21,27,28,35] and examined the $\tau-\Phi$ relationship of each individual PSII fluorescence component. Despite the large dispersion in the various results, the slow lifetime component shows a positive lifetime-axis intercept, similar to the one measured in this study (data not shown).

At first glance, we interpreted the positive lifetime-axis intercept as a time lag due to the energy transfer from an absorbing pigment to the emitting one. However, antenna pigments like carotenoids and Chl *a*/*b* cannot account for this phenomenon as the energy in the antenna is known to equilibrate with the PSII reaction center on the picosecond time scale [19,39,40].

Schreiber and Krieger [46] assumed that recombination fluorescence contributes significantly to the variable fluorescence upon Q_A reduction as originally hypothesized [47,48]. Based on this hypothesis, the positive extrapolation of the $\tau-\Phi$ relationship could be understood as a delayed emission related to excitation during the process of charge recombination. Experimental evidence favoring this hypotheses is, however, difficult to obtain because it is not easy to separate the prompt from the recombination fluorescence.

In order to explain the positive intercept of the $\tau-\Phi$ relationship, it was mandatory to simulate the variable fluorescence. We modeled its behavior in the framework of the three compartment model, introduced above, assuming first-order de-excitation processes with rate constants obtained from the published literature. The variable fluorescence was simulated by continuously varying the rate constant corresponding to the non-radiative dissipation pathway within the range of physiological values (Appendix B). This situation corresponds well to variable nonphotochemical quenching (NPQ) in the antenna. In this way, we obtained large variations of the total fluorescence, which are accompanied by changes of the different fluorescence components.

Two cases were taken into consideration with respect to the site of the NPQ: (i) the variable quenching was induced only in the main antenna (compartment (1)) and (ii) the variable quenching was induced simultaneously in the main antenna and the loosely connected compartment (compartment (3)). We found that both PSII nanosecond lifetime components exhibit almost linear $\tau-\Phi$ relationships during the whole induced variation (Fig. B2), irregardless of where NPQ was occurring. Moreover, the $\tau-\Phi$ relationship of the main long lifetime component exhibits a significant positive lifetime-axis intercept as does the measured T_3 component. However, it is important to note that only the case that takes into account quenching in the loosely connected compartment can explain the experimental data (Fig. B2B versus Fig. 4C).

Based on the evidence we have presented, we conclude that the significant positive lifetime-axis intercept of the $\tau-\Phi$ relationship of the T_3 component is a result of the compartmentation of the excitation energy in PSII antenna complexes.

4.4. The IP thermal phase of the fluorescence induction

In the companion paper, we investigated the pattern of the mean $\tau-\Phi$ relationship measured by PMF at 54 MHz. We proposed that a conformational change is responsible for the convex curvature observed during the IP thermal phase.

Our hypothesis was strongly supported by a transitory spectral change of the fluorescence during this phase.

The multi-frequency PMF results presented here show clearly that the curvature of the $\tau-\Phi$ relationship during the IP phase is an intrinsic feature of the long lifetime component T_3 (Fig. 3C). This component, which is the major contributor to the fluorescence signal during the IP phase, itself shows a strong convex curvature of the $\tau-\Phi$ relationship. On the other hand, the energy distribution between the two PSII components favors the T_3 component, whereas the T_2 component tends to decrease. It is very likely that all these results may be a consequence of the same phenomenon, namely the conformational change during the thermal phase.

Based on the kinetic model with three compartments, it appears clearly that the T_2 and T_3 components are not independent. This is consistent with the opposite variation of the T_2 and T_3 fluorescence yields during the IP phase (Fig. 3B), which suggests a physical interaction (energy exchange) between the pigment complexes at the origin of these lifetimes within the kinetic model.

It is worthwhile to note that both the positive lifetime-axis intercept and the curvature of the $\tau-\Phi$ relationship affect the same fluorescence component. It is thus very likely that the loosely connected pigment–protein complex is responsible for both effects. The conformational change invoked presumably involves this complex, perhaps either induced by/or itself inducing a modulation of the efficiency of the energy transfer to the main antenna. In the companion paper, we concluded that the conformational change must occur in the PSII core antenna complexes (CP43 and CP47) because the same effect (i.e., curvature of the $\tau-\Phi$ relationship) was observed in both wild-type barley and *chlorina* f2 mutant leaves.

In view of the recent results of Jennings et al. [44], it is possible that this pigment protein complex compartment is the CP47 complex, which appears to be loosely coupled with the peripheral antenna [49,50] and is responsible for the diffusion limited component of the overall trapping process. In addition, the approximately 15% fractional contribution of the loosely connected compartment to the total absorbed light (Appendix B), as found from the decomposition of the PMF data, agrees well with the pigment content of the CP47 complex.

Boussac et al. [51] have studied the effect of the strong oxidant irridate (K_2IrCl_6) on the fluorescence properties of PSII enriched particles (BBY) and isolated LHCII. They showed that the fluorescence lifetime components are differently affected. The picosecond component is quite insensitive, while the two nanosecond components are strongly quenched. They concluded that the addition of irridate acts on the antenna pigments level via two NPQ mechanisms, one static and the other dynamic, which do not inactivate the charge separation. More important, quenching induced by increasing concentrations of irridate affected the $\tau-\Phi$ relationships in a similar manner as the $T_2-\Phi_2$ and $T_3-\Phi_3$ relationships (Fig. 3C).

Recently, Moya et al. [52] analyzed the picosecond time-resolved kinetics of fluorescence decay from four purified components of the PSII antenna (LHCII, CP29, CP26 and CP24) related to NPQ. They concluded that two factors modulate the quenching of Chl fluorescence in LHCII proteins, namely intrasubunit conformational change and intersubunit interactions within the lipid membrane. LHCII proteins binding zeaxanthin underwent static quenching. Upon their incorporation into liposomes, another kind of quenching was observed, resulting from protein–protein interactions. The latter quenching affected both the fluorescence yield and lifetime of LHCII proteins in vivo.

These results, obtained in vitro, show the diversity and complexity of the variations of PSII fluorescence components, both in lifetime and yield, that are associated with pigment–protein conformational modifications. Our results show that some of the features presented above are still present in vivo. They are induced in dark-adapted material during the first second of illumination with low actinic light and are associated with a transitory conformational change. This change must be different from the structural changes of LHCII observed in high actinic light and induced by the buildup of ΔpH [53–55].

4.5. The PS phase of the fluorescence induction

The results of the multi-frequency PMF analysis show that the $\tau-\Phi$ relationship of both T_2 and T_3 fluorescence components are linear during the PS phase of fluorescence induction (Fig. 4C). The PS phase is dominated by the reoxidation of Q_A^- and the development of NPQ (mainly, the energy-dependent quenching qE), which roughly exhibits a dynamic quenching behavior for both PSII fluorescence components [41,56], and therefore similarly affects the quantum yield and lifetime. The extrapolation of the $T_3-\Phi_3$ relationship to the lifetime axis gave a positive value (1 ns), similar to that obtained during the OI phase. As previously stated, we interpret this positive extrapolation as a delay introduced by the compartmentation of the excitation energy between the main antenna and a loosely connected antenna compartment.

Simulations of the variable fluorescence with our kinetic model showed good agreement with experimental data. The fluorescence was modulated by continuously varying the thermal dissipation pathway of the antenna excited states (Appendix B). It is important to note that the variable quenching induced in this way simulates quite well the quenching developed during the PS phase of the fluorescence induction. Although we considered two possible cases related to the site of the quenching simulated in the PSII antenna, we found that only the quenching associated with the loosely connected compartment can account for the experimental data (Fig. B2B versus Fig. 4C). This new result suggests that the loosely connected compartment is involved both in the conformational change, previously described, as well as in the mechanisms of NPQ.

Considering the mean $T_m-\Phi$ relationship, we emphasize that its linearity during the PS phase is a consequence of the linear $\tau-\Phi$ relationship of each PSII component. This result demonstrates that in the absence of a disturbance, i.e. a conformational change, the $\tau-\Phi$ relationship should be linear. The negative extrapolation of the $T_m-\Phi$ relationship on the lifetime axis is a consequence of two antagonistic facts. One is the large positive extrapolation of the $T_3-\Phi_3$ relationship. The other is the negative extrapolation of the $T_2-\Phi_2$ relationship and the contribution of the short lifetime component of PSI. It was already shown that the extrapolation close to the origin of the mean $T_m-\Phi$ relationship in leaves largely depends on the PSI contribution to the fluorescence emission [35,36]. This is in agreement with previous reports on algae, chloroplasts [24,57] and leaves [41,56].

The fact that the $T_m-\Phi$ relationship during the PS phase can be linear considering the heterogeneity of Chl *a* fluorescence is a remarkable result. This feature allows one to estimate the Chl *a* fluorescence yield in vivo by measuring the fluorescence lifetime, as previously proposed [58]. Moreover, any deviation from the linearity of the $\tau-\Phi$ relationship during the PS phase has been recently shown to be a sensitive indicator for various environmental stress conditions [35,36] and consequently for the plant physiology.

5. Concluding remarks

On the basis of the multi-frequency PMF results, we can reconcile two apparently antagonistic aspects of Chl *a* fluorescence in vivo: it is heterogeneous with respect to the kinetic structure (several lifetime components) and homogeneous with respect to average quantities (quasi-linear mean $\tau-\Phi$ relationship).

We have shown that a loosely connected pigment complex, which is assumed to be the CP47 complex, plays a specific role with respect to the structure and function of PSII: (i) it explains the heterogeneity of the PSII fluorescence lifetime as a compartmentation of excitation energy in the antenna, (ii) it is the site of a conformational change in the first second of illumination, and (iii) it is involved in the mechanisms of NPQ developed during the slow PS phase of the fluorescence induction.

Multi-frequency PMF proves to be a new and powerful methodological approach in the analysis of variable fluorescence, showing the possibility of filling the gap between fluorescence analysis and molecular composition of the photosynthetic apparatus under different physiological conditions.

Acknowledgements

We thank Dr. Z.G. Cerovic, Dr. J. Lavergne, Dr. J.-M. Ducruet, Dr. F. Morales, Dr. J. Cavender-Bares, Dr. G. Parlant and Dr. D. Parent for stimulating discussions and useful suggestions on the manuscript. Thanks are also due to Dr. Y. Goulas and Dr. M. Bergher for helpful discussions. This work was supported by CNRS through the GDR #1536. N. Moise gratefully acknowledges the "Réseau Formation-Recherche Franco-Roumain" #97P4701, the LURE and the CNRS for their financial support.

Appendix A. Multi-frequency PMF data analysis

The analysis of frequency-domain data has already been described in detail [59–64]. However, the use of the frequency-domain analysis is less intuitive than the time-domain analysis. Moreover, we have applied the multi-frequency PMF analysis not under steady state conditions but during periods of rapid changes in the fluorescence, making the interpretation of the data more difficult. We thus briefly describe below the decomposition procedure of the multi-frequency PMF data. We postulate a multi-exponential model for the heterogeneous fluorescence emission from photosynthetic systems as:

$$F(t)=\sum_{i=1}^{n}\alpha_i e^{-t/\tau_i} \tag{A1}$$

where τ_i represents the individual lifetimes and α_i the pre-exponential factors. The fractional contribution of each component to the total steady-state intensity emission, f_i, is given by:

$$f_i=\frac{\alpha_i\tau_i}{\sum_j \alpha_j\tau_j}=\frac{\Phi_i}{\Phi_{\text{total}}} \tag{A2}$$

The mean fluorescence lifetime is related to the multi-exponential parameters of the physical model according to [65]:

$$\tau_{\text{mean}}=\frac{\int_0^\infty t\cdot F(t)\mathrm{d}t}{\int_0^\infty F(t)\mathrm{d}t}=\frac{\sum_{i=1}^{n}\alpha_i\tau_i^2}{\sum_{i=1}^{n}\alpha_i\tau_i}=\sum_{i=1}^{n}f_i\tau_i \tag{A3}$$

By introducing the sine (P_ω) and cosine (Q_ω) transforms of the impulse response, at the circular frequency ω, as

$$P_\omega=\sum_{i=1}^{n}\frac{f_i\omega\tau_i}{1+\omega^2\tau_i^2}$$

$$Q_\omega=\sum_{i=1}^{n}\frac{f_i}{1+\omega^2\tau_i^2} \tag{A4}$$

one may predict the frequency-dependent values for phase and modulation as

$$\phi_{c\omega}=\tan^{-1}(P_\omega/Q_\omega)$$

$$m_{c\omega}=(P_\omega^2+Q_\omega^2)^{1/2} \tag{A5}$$

and for the phase τ_p and modulation τ_m lifetimes, respectively, as:

$$\tau_p^{c\omega} = \frac{1}{\omega}\tan(\phi_{c\omega})$$

$$\tau_m^{c\omega} = \frac{1}{\omega}(1/m_{c\omega}^2 - 1)^{1/2} \quad \text{(A6)}$$

By measuring at several modulation frequencies, a set of nonlinear equations is obtained according to Eq. (A6). Assuming an a priori number of discrete components in the heterogeneous fluorescence emission, the lifetime and the fractional contribution of each component can be determined through nonlinear least-squares analysis (NLLS) [66]. A very comprehensive review of the exponential analysis of physical phenomena was written by Istratov and Vyvenko [67]. Based on the χ^2 criterion, the NLLS procedure minimizes the squared deviations between the observed and expected phase and modulation values, weighted by standard deviations of the measured phase and modulation values. We used the Marquardt procedure described by Bevington [68] for the minimization of χ^2. Due of its real physical significance in the interpretation of fluorescence induction in leaves, we chose to work with the PMF lifetimes (Eq. (A6)) instead of the phase and modulation values (Eq. (A5)). Therefore, we used the following expression of χ^2:

$$\chi^2 = \sum_{\omega}\frac{1}{\sigma_{\tau p\omega}^2}(\tau_p - \tau_p^{c\omega})^2 + \sum_{\omega}\frac{1}{\sigma_{\tau m\omega}^2}(\tau_m - \tau_m^{c\omega})^2 \quad \text{(A7)}$$

where τ_p, τ_m are the measured lifetimes and $\tau_p^{c\omega}$, $\tau_m^{c\omega}$ are the calculated lifetimes at the indicated frequency. $\sigma_{\tau p\omega}$ and $\sigma_{\tau m\omega}$ refer to the standard deviations of the measured PMF lifetimes under the chosen experimental conditions.

The goodness of fit was judged from the value of reduced χ^2,

$$\chi_R^2 = \frac{\chi^2}{v} = \frac{\chi^2}{2N - p} \quad \text{(A8)}$$

where $v = 2N - p$ is the number of degrees of freedom, N is the number of frequencies and p is the number of unknown parameters. Contrary to the TCSPC data analysis, statistical information (e.g. a Poisson distribution) about the random errors in phase and modulation is not available. For all analyses, the uncertainties in the phase and modulation were taken as 0.2° and 0.005, respectively, which represent the maximal errors of our instrument. Generally, the errors depend on frequency, but, more importantly, they depend on the fluorescence light intensity. Therefore, the absolute value of χ_R^2 is not necessarily near unity, but this is less relevant when χ_R^2 is calculated for a continuously varying signal like the fluorescence induction.

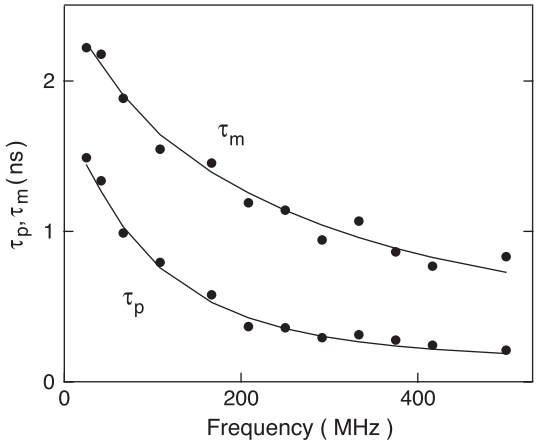

Fig. A1. The best fit (solid curves) of simulated τ_p and τ_m lifetime data (solid points) at 12 modulation frequencies ranging from 30 to 500 MHz for a physical model with three exponential terms assumed to be 0.1 ns (30% fractional contribution), 1.2 ns (30%) and 3 ns (40%). A random noise of about 10% was added to both τ_p and τ_m. The parameters found upon data analysis of 25 replicates were 0.104 ± 0.021 ns ($30.31 \pm 0.93\%$), 1.193 ± 0.051 ns ($30.7 \pm 1.7\%$) and 3.08 ± 0.069 ns ($39.4 \pm 2.2\%$).

The program for multi-frequency PMF data analysis was written using the HP Basic 7.0 (Hewlett Packard, USA) language. We tested the decomposition program on the basis of simulated phase and modulation data for several heterogeneous systems. We generally assumed a constant level of random errors, independent of frequency, phase angle or modulation. Fig. A1 shows the best fit of simulated phase and modulation lifetime data at 12 modulation frequencies ranging from 30 to 500 MHz for a synthetic model with three exponential terms having lifetimes of 0.1 ns (30% fractional contribution), 1.2 ns (30%) and 3 ns (40%). Errors of about 10% of the highest value of the PMF lifetimes were added. The parameters found upon data analysis of 25 replicates were 0.104 ± 0.021 ns ($30.31 \pm 0.93\%$), 1.193 ± 0.051 ns ($30.7 \pm 1.7\%$) and 3.08 ± 0.069 ns ($39.4 \pm 2.2\%$), thus validating our decomposition procedure.

Appendix B. Model of compartmentation of excitation energy in PSII antenna

This model is an extension of the well-known RRP model [19,39,40] that assumes a rapid equilibrium of the excitation energy between PSII pigments and the reaction center, and a reversibility of the charge separation. In order to account for the PSII fluorescence lifetime heterogeneity, we introduced an additional PSII kinetic compartment as previously proposed [38]. Accordingly, this model corresponds to a three compartment kinetic scheme and is characterized by a set of several rate constants (Fig. B1). The mathematical formulation of the model results in a system of three linear differential equations. The model predicts three PSII fluorescence lifetime components, with two of them in the nanosecond time range. It is important to

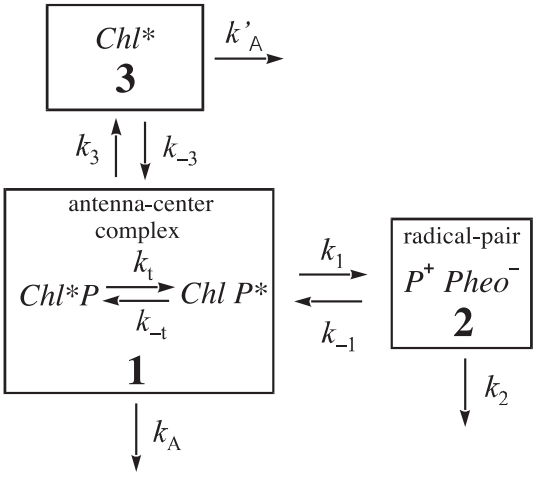

Fig. B1. Scheme of the three compartments kinetic model of PSII energy migration, modified from the original RRP model. (1) is the main antenna compartment, (2) is the radical pair compartment, (3) is the loosely connected compartment. When compartments (1) and (3) are tightly connected to form a single pigments pool, this model becomes the original RRP model. k_t and k_{-t}, called trapping and detrapping rate constants, are assumed to be too fast to be explicitly considered in the model. k_1 and k_{-1} describe the primary charge separation and charge recombination processes, respectively. k_2 describes the overall decay processes of the primary radical pair (e.g., the charge stabilization). k_A and k'_A include both the radiative (fluorescence) and radiationless antenna deactivation processes. k_3 and k_{-3} are the rate constants of the excitation energy exchange between the loosely compartment and the main antenna.

stress that both fluorescent pigment compartments, (1) and (3), exhibit three exponential fluorescence decays with the same lifetimes (T_1, T_2 and T_3) but with different amplitudes. It is thus evident that none of the measured lifetime components can be attributed exclusively to a single process or as proceeding from a single compartment. Lifetimes and amplitudes are, in fact, complex functions of all rate constants and cross-section parameters of each compartment.

Searching for an accurate description of the third compartment, a mathematical inversion of the kinetic model was developed under the Mathematica 4.0 programming environment (Wolfram Research, USA). By introducing into the model the experimental PSII fluorescence parameters, lifetimes and yields, obtained from the multi-frequency PMF analysis at the F_p maximal fluorescence level (data from Table 1), we can determine the rate constants characterizing the energy exchange between the compartment in question and the main antenna.

k_A and k'_A represent the deactivation rate constants of the antenna excited states and contain both the radiative decay (fluorescence) and the radiationless decay (thermal dissipation). These rate constants were fixed to a value of 0.25 ns^{-1} derived from the fluorescence lifetime measured in isolated LHCII [69]. For the other rate constants, which characterize the PSII acceptor-side kinetics, we used values from the RRP model literature: $k_1 = 1.5$ ns^{-1}, $k_{-1} = 2.30$ ns^{-1} and $k_2 = 2.9$ ns^{-1} [3,19,38,40,41,69]. A nonlinear Levenberg–Marquardt algorithm routine in Mathematica 4.0 was used to retrieve the unknown parameters of the system concerning the third pigment compartment: k_3, k_{-3} and its fractional contribution related to the total absorbed light.

Upon minimization of the sum of the squared weighted residuals over all data points, we found that compartment (3) accounts for approximately 15% of the total light absorption, whereas compartment (1), corresponding to the main antenna, has a contribution of 85%. Concerning the rate constants that characterize the energy exchange between compartments (3) and (1), we found two similar values, $k_3 = 0.26$ ns^{-1} and $k_{-3} = 0.2235$ ns^{-1}, very close to the values assumed for k_A and k'_A. The values obtained for k_3 and k_{-3} clearly indicate that the new compartment is loosely connected to the main antenna and that energy tends to accumulate in the third compartment. In addition, we found that the fast PSII fluorescence component (T_1) is characterized by a lifetime of about 150 ps and provides a small fractional contribution of about 1.5% of the total PSII emission.

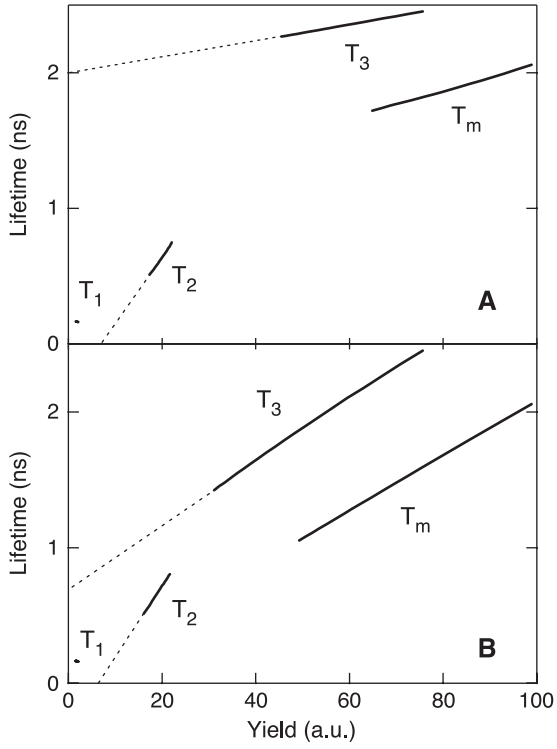

Fig. B2. Simulation of the variable fluorescence within the framework of the PSII kinetic model with three compartments. Considering initially PSII at the maximal fluorescence level, the variable fluorescence was simulated by a variable NPQ induced in the antenna by continuously varying the k_A and k_A' rate constants, while the values of other rate constants of the system were held fixed. The parameters that describe compartment (3) were previously found: $k_3 = 0.26$ ns^{-1}, $k_{-3} = 0.2235$ ns^{-1} and 15% from the total light absorption. Two cases were considered: (A) only k_A was varied between 0.25 and 1.2 ns^{-1}, (B) k_A was varied between 0.25 and 1.2 ns^{-1}, while k'_A was varied between 0.25 and 0.55 ns^{-1}. The relationship between the fluorescence lifetime and yield was analyzed for each PSII lifetime component (T_1, T_2 and T_3). The mean fluorescence lifetime (T_m) is plotted versus the total yield.

B.1. Simulation of the PSII variable fluorescence

With the PSII antenna system fully characterized at the maximal fluorescence level, we added a variable non-radiative dissipation pathway for the antenna-excited states (i.e., a variable NPQ) in order to simulate the variation of the fluorescence. We considered two cases. First, we quenched only the excited states of the main antenna (compartment (1)) by varying continuously k_A within the range of physiological values between 0.25 and 1.2 ns^{-1}. Variation of k_A induced variations of the three PSII fluorescence components, both in lifetime and yield, and allows the analysis of the $\tau-\Phi$ relationship of each fluorescence lifetime component. Fig. B2A summarizes the results obtained when variable quenching of the main antenna was simulated. It is important to note that the $\tau-\Phi$ relationships of both nanosecond components, T_2 and T_3, are almost linear. Consequently, the $\tau-\Phi$ relationship of the mean T_m lifetime is also linear. However, we observed that neither the extent of variation nor the value of the $\tau-\Phi$ relationship extrapolation (2 ns for T_3 and 1.2 ns for T_m) corresponds to experimental data (Fig. B2A versus Fig. 4C).

In a second case, we added an additional variable quenching at the level of the excited states of compartment (3) and we varied simultaneously both k_A' (from 0.25 to 0.55 ns^{-1}) and k_A (from 0.25 to 1.2 ns^{-1}). The results are shown in Fig. B2B. We still obtained almost linear $\tau-\Phi$ relationships for T_2, T_3 and T_m. The T_2 component is not affected by the new quenching, since behavior identical to the first case is observed. On the contrary, the T_3 component is largely affected. The linear $\tau-\Phi$ relationship of T_3 extrapolates now to about 0.7 ns. In addition, the extent of the variation is accurately reproduced. In conclusion, this behavior agrees well with experimental data (Fig. B2B versus Fig. 4C).

References

[1] M. Hodges, I. Moya, Time-resolved chlorophyll fluorescence studies of photosynthetic membranes: resolution and characterisation of four kinetic components, Biochim. Biophys. Acta 849 (1986) 193–202.

[2] G. Schmuck, I. Moya, Time-resolved chlorophyll fluorescence spectra of intact leaves, Remote Sens. Environ. 47 (1994) 72–76.

[3] S. Vasil'ev, D. Bruce, Nonphotochemical quenching of excitation energy in photosystem II. A picosecond time-resolved study of the low yield of chlorophyll *a* fluorescence induced by single-turnover flash in isolated spinach thylakoids, Biochemistry 37 (1998) 11046–11054.

[4] A.R. Holzwarth, J. Wendler, W. Haehnel, Time-resolved picosecond fluorescence spectra of the antenna chlorophylls in *chlorella vulgaris*. Resolution of Photosystem I fluorescence, Biochim. Biophys. Acta 807 (1985) 155–167.

[5] I. Moya, P. Sebban, W. Haehnel, Lifetime of excited states and quantum yield of chlorophyll *a* fluorescence in vivo, in: Govindjee, J. Amesz, D.C. Fork (Eds.), Light Emission by Plants and Bacteria, Academic Press, Orlando, Florida, 1986, pp. 161–190.

[6] T.A. Roelofs, C.-H. Lee, A.R. Holzwarth, Global target analysis of picosecond chlorophyll fluorescence kinetics from pea chloroplasts. A new approach to the characterisation of the primary processes in photosystem II α- and β-units, Biophys. J. 61 (1992) 1147–1163.

[7] A.R. Holzwarth, Fluorescence lifetimes in photosynthetic systems, Photochem. Photobiol. 43 (1986) 707–725.

[8] A.R. Holzwarth, Excited-state kinetics in chlorophyll systems and its relationship to the functional organization of the photosystems, in: H. Scheer (Ed.), Chlorophylls, CRC Handbook, CRC Press, Boca Raton, 1991, pp. 1125–1151.

[9] M. Hodges, I. Moya, Modification of room-temperature picosecond chlorophyll fluorescence kinetics in photosystem-II-enriched particles by photochemistry, Biochim. Biophys. Acta 892 (1987) 42–47.

[10] M. Hodges, I. Moya, Time-resolved chlorophyll fluorescence studies on pigment–protein complexes from photosynthetic membranes, Biochim. Biophys. Acta 935 (1988) 41–52.

[11] A. Melis, G.E. Guenther, P.J. Morrissey, M.L. Ghirardi, Photosystem II heterogeneity in chloroplasts, in: H.K. Lichtenthaler (Ed.), Applications of Chlorophyll Fluorescence, Kluwer Academic Publishing, Dordrecht, The Netherlands, 1988, pp. 33–43.

[12] J. Cao, Govindjee, Chlorophyll *a* fluorescence transient as an indicator of active and inactive photosystem-II in thylakoid membranes, Biochim. Biophys. Acta 1015 (1990) 180–188.

[13] J. Lavergne, E. Leci, Properties of inactive Photosystem-II centers, Photosynth. Res. 35 (1993) 323–343.

[14] Govindjee, Photosystem-II heterogeneity: the acceptor side, Photosynth. Res. 25 (1990) 151–160.

[15] A. Melis, Dynamics of photosynthetic membrane composition and function, Biochim. Biophys. Acta 1058 (1991) 87–106.

[16] J. Lavergne, J.-M. Briantais, Photosystem-II heterogeneity, in: D.R. Ort, C.F. Yocum (Eds.), Oxygenic Photosynthesis: The Light Reactions, Kluwer Academic Publishing, Dordrecht, 1996, pp. 265–287.

[17] S.J. Berens, J. Scheele, W.L. Butler, D. Madge, Time-resolved fluorescence studies of spinach chloroplasts—Evidence for the heterogeneous bipartite model, Photochem. Photobiol. 42 (1985) 51–57.

[18] W.L. Butler, D. Magde, S.J. Berens, Fluorescence lifetimes in the bipartite model of the photosynthetic apparatus with heterogeneity in photosystem II, Proc. Natl. Acad. Sci. U. S. A. 80 (1983) 7510–7514.

[19] H. Dau, Molecular mechanisms and quantitative models of variable Photosystem-II fluorescence, Photochem. Photobiol. 60 (1994) 1–23.

[20] N.E. Geacintov, J. Breton, Energy transfer and fluorescence mechanisms in photosynthetic membranes, CRC Crit. Rev. Plant Sci. 5 (1987) 1–44.

[21] W. Haehnel, J.A. Nairn, P. Reisberg, K. Sauer, Picosecond fluorescence kinetics and energy transfer in chloroplasts and algae, Biochim. Biophys. Acta 680 (1982) 161–173.

[22] C. Vernotte, A.L. Etienne, J.-M. Briantais, Quenching of the system II chlorophyll fluorescence by the plastoquinone pool, Biochim. Biophys. Acta 545 (1979) 519–527.

[23] J. Lavorel, A study of chlorophyll fluorescence in vivo by a flow method, Photochem. Photobiol. 4 (1965) 819–828.

[24] J.-M. Briantais, H. Merkelo, Govindjee, Lifetime of the excited state (τ) in vivo: III. Chlorophyll during fluorescence induction in *Chlorella pyrenoidosa*, Photosynthetica 6 (1972) 133–141.

[25] I. Moya, Durée de vie et rendement de fluorescence de la chlorophylle in vivo. Leur relation dans différents modèles d'unités photosynthétiques, Biochim. Biophys. Acta 368 (1974) 214–227.

[26] I. Moya, Application de la fluorimétrie de phase à l'étude de la durée de vie et du rendement de la fluorescence de la chlorophylle in vivo. PhD thesis, Université de Paris XI, Orsay 1979.

[27] A. Krieger, I. Moya, E. Weis, Energy-dependent quenching of chlorophyll a fluorescence: effect of pH on stationary fluorescence and picosecond-relaxation kinetics in thylakoid membranes and Photosystem II preparations, Biochim. Biophys. Acta 1102 (1992) 167–176.

[28] I. Moya, M. Hodges, J.-C. Barbet, Modification of room-temperature picosecond chlorophyll fluorescence kinetics in green algae by photosystem II trap closure, FEBS Lett. 198 (1986) 256–262.

[29] R.D. Spencer, G. Weber, Measurements of subnanosecond fluorescence lifetimes with a cross-correlation phase fluorometer, Ann. N.Y. Acad. Sci. 158 (1969) 361–376.

[30] E. Gratton, D.M. Jameson, N. Rosato, G. Weber, Multifrequency cross-correlation phase fluorometer using synchrotron radiation, Rev. Sci. Instrum. 55 (1984) 486–494.
[31] J.R. Lakowicz, A. Balter, Theory of phase-modulation fluorescence spectroscopy for excited-state processes, Biophys. Chem. 16 (1982) 99–115.
[32] G. Weber, Resolution of the fluorescence lifetimes in a heterogeneous system by phase and modulation measurements, J. Phys. Chem. 85 (1981) 949–953.
[33] W. Haehnel, A.R. Holzwarth, J. Wendler, Picosecond fluorescence kinetics and energy transfer in the antenna chlorophylls of green algae, Photochem. Photobiol. 37 (1983) 435–443.
[34] G. Agati, Z.G. Cerovic, I. Moya, The effect of decreasing temperature up to chilling values on the in vivo F685/F735 chlorophyll fluorescence ratio in *Phaseolus vulgaris* and *Pisum sativum*: the role of the Photosystem I contribution to the 735 nm fluorescence band, Photochem. Photobiol. 72 (2000) 75–84.
[35] S. Apostol, J.-M. Briantais, N. Moise, Z.G. Cerovic, I. Moya, Photoinactivation of the photosynthetic electron transport chain by accumulation of over-saturating light pulses given to dark-adapted pea leaves, Photosynth. Res. 67 (2001) 215–227.
[36] F. Morales, N. Moise, R. Quilez, A. Abadia, J. Abadia, I. Moya, Iron deficiency interrupts energy transfer from a disconnected part of the antenna to the rest of Photosystem II, Photosynth. Res. 70 (2001) 207–220.
[37] E. Pfundel, Estimating the contribution of Photosystem I to total leaf chlorophyll fluorescence, Photosynth. Res. 56 (1998) 185–195.
[38] J.-M. Briantais, J. Dacosta, Y. Goulas, J.-M. Ducruet, I. Moya, Heat-stress induces in leaves an increase of the minimum level of chlorophyll fluorescence, Fo: a time resolved analysis, Photosynth. Res. 46 (1996) 189–196.
[39] G.H. Schatz, H. Brock, A.R. Holzwarth, Picosecond kinetics of fluorescence and absorbance changes in photosystem II particles excited at low photon density, Proc. Natl. Acad. Sci. U. S. A. Biophys. 84 (1987) 8414–8418.
[40] G.H. Schatz, H. Brock, A.R. Holzwarth, Kinetic and energetic model for the primary processes in Photosystem II, Biophys. J. 54 (1988) 397–405.
[41] Y. Goulas, Teledétection de la fluorescence des couverts végétaux: Temps de vie de la fluorescence chlorophyllienne et fluorescence bleue, PhD thesis, Université de Paris XI, Orsay 1992.
[42] R.C. Jennings, R. Bassi, F.M. Garlaschi, P. Dainese, G. Zucchelli, Distribution of the chlorophyll spectral forms in the chlorophyll–protein complexes of Photosystem II antenna, Biochemistry 32 (1993) 3203–3210.
[43] R.C. Jennings, G. Zucchelli, L. Finzi, F.M. Garlaschi, Spectral heterogeneity and energy equilibration in higher plant photosystems, in: R.C. Jennings, G. Zucchelli, F. Ghetti, G. Colombetti (Eds.), Light as an Energy Source and Information Carrier in Plant Physiology, Plenum, New York, 1996, pp. 65–74.
[44] R.C. Jennings, E. Gianluca, F.M. Garlaschi, S. Santabarbara, Z. Giuseppe, Selective quenching of the fluorescence of core chlorophyll–protein complexes by photochemistry indicates that Photosystem II is partly diffusion limited, Photosynth. Res. 66 (2000) 225–233.
[45] S. Vasil'ev, P. Orth, A. Zouni, T.G. Owens, D. Bruce, Excited-state dynamics in Photosystem II: insights from the X-ray crystal structure, Proc. Natl. Acad. Sci. U. S. A. 98 (2001) 8602–8607.
[46] U. Schreiber, A. Krieger, Two fundamentally different types of variable chlorophyll fluorescence in vivo, FEBS Lett. 397 (1996) 131–135.
[47] V.V. Klimov, A.V. Klevanik, V.A. Shuvalov, A.A. Krasnovsky, Reduction of pheophytin in the primary light reaction of Photosystem II, FEBS Lett. 82 (1977) 183–186.
[48] V.A. Shuvalov, V.V. Klimov, E. Dolan, W.W. Parson, B. Ke, Nanosecond fluorescence and absorbance changes in Photosystem II at low redox potential, FEBS Lett. 118 (1980) 279–282.
[49] E.J. Boekema, H. Van Roon, F. Calkoen, R. Bassi, J.P. Dekker, Multiple types of association of Photosystem II and its light-harvesting antenna in partially solubilized Photosystem II membranes, Biochemistry 38 (1999) 2233–2239.
[50] J.P. Dekker, R. van Grondelle, Primary charge separation in Photosystem II, Photosynth. Res. 63 (2000) 195–208.
[51] A. Boussac, M. Hodges, J.M. Briantais, I. Moya, The quenching characteristics of potassium iridic chloride and their meaning for the origin of chlorophyll fluorescence components, Photosynth. Res. 20 (1989) 173–189.
[52] I. Moya, M. Silvestri, O. Vallon, G. Cinque, R. Bassi, Time-resolved fluorescence analysis of the Photosystem II antenna proteins in detergent micelles and liposomes, Biochemistry 40 (2001) 12552–12561.
[53] P. Horton, A.V. Ruban, D. Rees, G. Noctor, A.A. Pascal, A. Young, Control of the light harvesting function of chloroplast membranes by aggregation of the LHCII chlorophyll protein complex, FEBS Lett. 292 (1991) 1–4.
[54] A.V. Ruban, A.J. Young, P. Horton, Induction of nonphotochemical energy dissipation and absorbance changes in leaves—evidence for changes in the state of the light-harvesting system of Photosystem II in vivo, Plant Physiol. 102 (1993) 741–750.
[55] P. Horton, A.V. Ruban, R.G. Walters, Regulation of light harvesting in green plants, Annu. Rev. Plant Physiol. Plant Mol. Biol. 47 (1996) 655–684.
[56] B. Genty, Y. Goulas, B. Dimon, G. Peltier, J.-M. Briantais, I. Moya, Modulation of efficiency of primary conversion in leaves, mechanisms involved at PS2, in: N. Murata (Ed.), Research in Photosynthesis, Kluwer Academic Publishing, Dordrecht, The Netherlands, 1992, pp. 603–610.
[57] L.A. Tumerman, E.M. Sorokin, Fotosinteticheskaya edinitsa: "fizicheskaya" ili "statisticheskaya" model? (The photosynthetic unit: a "physical" or "statistical" model? Mol. Biol. 1 (1967) 628–638.
[58] I. Moya, Y. Goulas, F. Morales, L. Camenen, G. Guyot, G. Schmuck, Remote sensing of time-resolved chlorophyll fluorescence and backscattering of the laser excitation by the vegetation, EARSeL J. Adv. Remote Sens. 3 (1995) 188–197.
[59] D. Eaton, Recommended methods for fluorescence decay analysis, Pure Appl. Chem. 62 (1990) 1632–1648.
[60] E. Gratton, M. Limkeman, Resolution of mixtures of fluorophores using variable-frequency phase and modulation data, Biophys. J. 46 (1984) 479–486.
[61] J.R. Lakowicz, I. Gryczynski, Frequency-domain fluorescence spectroscopy, in: J.R. Lakowicz (Ed.), Topics in Fluorescence Spectroscopy, volume 1, Techniques, Plenum, New York, 1991, pp. 293–335.
[62] J.M. Shaver, L.B. McGown, Maximum entropy method for frequency domain fluorescence lifetime analysis: 1. Effects of frequency range and random noise, Anal. Chem. 68 (1996) 9–17.
[63] J.M. Shaver, L.B. McGown, Maximum entropy method for frequency domain fluorescence lifetime analysis: 2. Timing, mismatched intensity, and reference lifetime errors, Anal. Chem. 68 (1996) 611–620.
[64] J.R. Lakowicz, G. Laczko, H. Cherek, E. Gratton, M. Limkeman, Analysis of fluorescence decay kinetics from variable-frequency phase shift and modulation data, Biophys. J. 46 (1984) 463–477.
[65] J.R. Lakowicz, H. Szmacinski, Imaging applications of time-resolved fluorescence spectroscopy, in: X.F. Wang, B. Herman (Eds.), Fluorescence Imaging Spectroscopy and Microscopy, vol. 137, Wiley, NY, 1996, pp. 273–311.
[66] M. Straume, S.G. Frasier-Cadoret, M.L. Johnson, Least-squares analysis of fluorescence data, in: J.R. Lakowicz (Ed.), Topics in Fluorescence Spectroscopy, volume 2, Principles, Plenum, New York, 1991, pp. 177–240.
[67] A.A. Istratov, O.F. Vyvenko, Exponential analysis in physical phenomena, Rev. Sci. Instrum. 70 (1999) 1233–1257.
[68] P.R. Bevington, Data Reduction and Error Analysis for the Physical Sciences, McGraw-Hill, New York, 1969.
[69] R. Bassi, M. Silvestri, P. Dainese, I. Moya, G.M. Giacometti, Effects of a non-ionic detergent on the spectral properties and aggregation state of the light-harvesting chlorophyll a/b protein complex (LHCII), J. Photochem. Photobiol. B Biol. 9 (1991) 335–354.